Supplementary figures

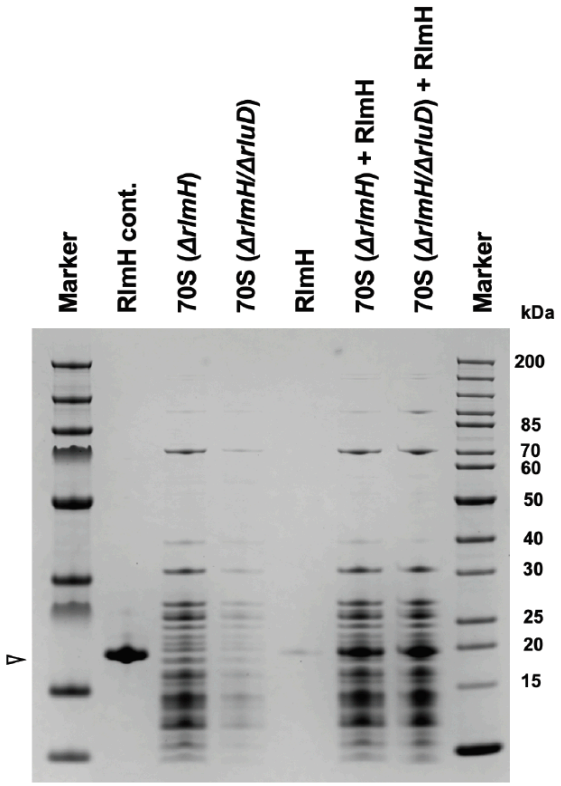

Figure S1. Ribosome-dependent co-pelleting of RlmH through sucrose cushion. Recombinant RlmH (pre-incubated with SAH) was incubated with 70S ribosomes isolated from *ΔrlmH* and *ΔrlmH/ΔrluD* strains and layered onto sucrose cushion for ultracentrifugation as described in materials and methods. Pellets were resuspended and analyzed by SDS-PAGE. Purified RlmH protein was used as a control.

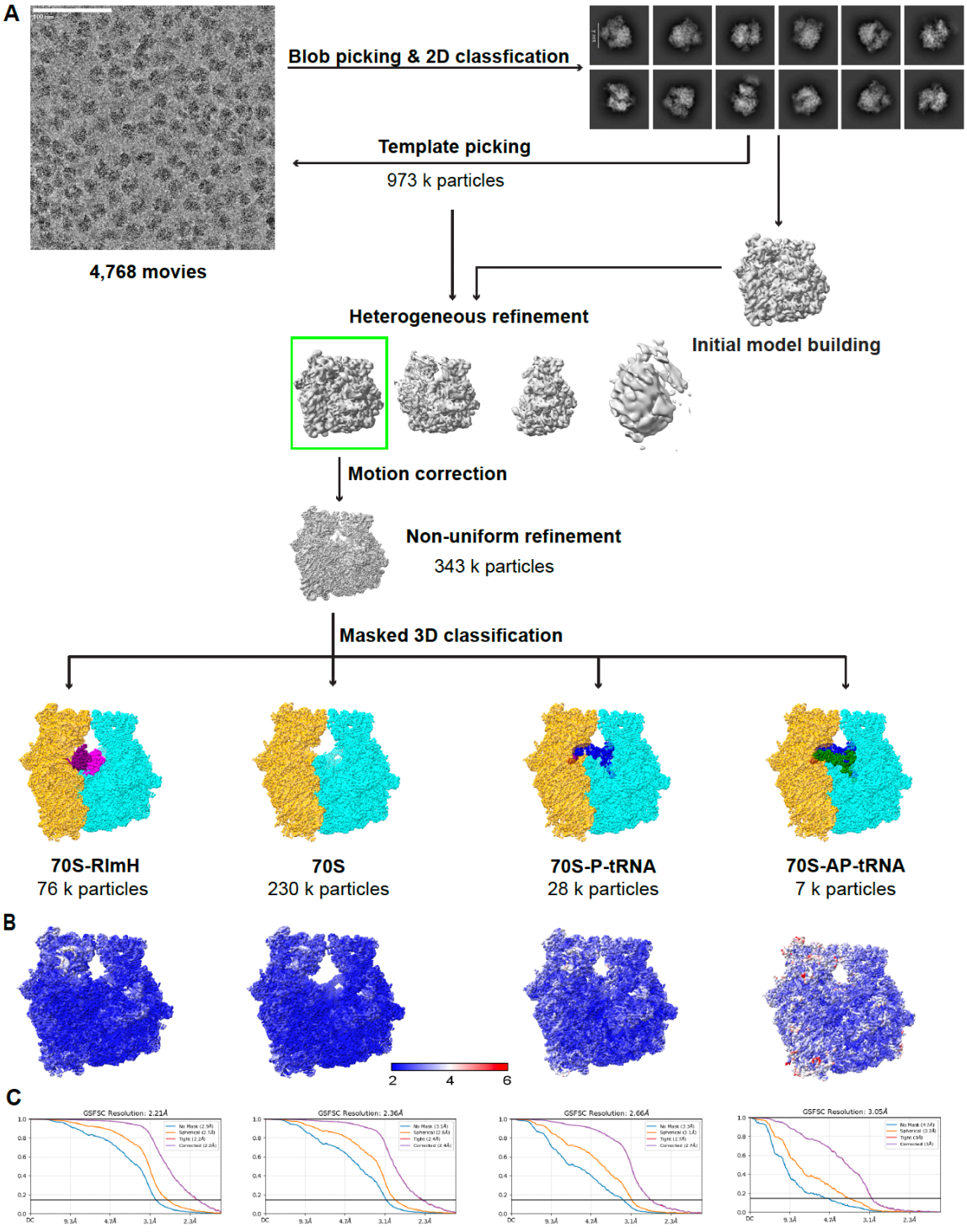

Figure S2. Cryo-EM data processing of 70S ribosomes from the *ΔrlmH/ΔrluD* strain. A) Overview of the cryo-EM data processing workflow for 70S ribosomes purified from the ΔrlmH/ΔrluD strain. Particles were subjected to iterative 2D classification followed by heterogeneous refinement. The selected particles were subsequently classified into four major structural states based on tRNA

occupancy and the presence of density corresponding to RlmH. Representative raw micrographs and selected 2D class averages are shown. The number of particles contributing to each reconstruction is indicated. **B)** Local resolution maps of the final cryo-EM reconstructions, with the corresponding resolution scale shown in the center. **C)** Gold-standard Fourier shell correlation (FSC) curves for the final 3D reconstructions. Overall resolutions were estimated using the gold-standard FSC criterion at 0.143.

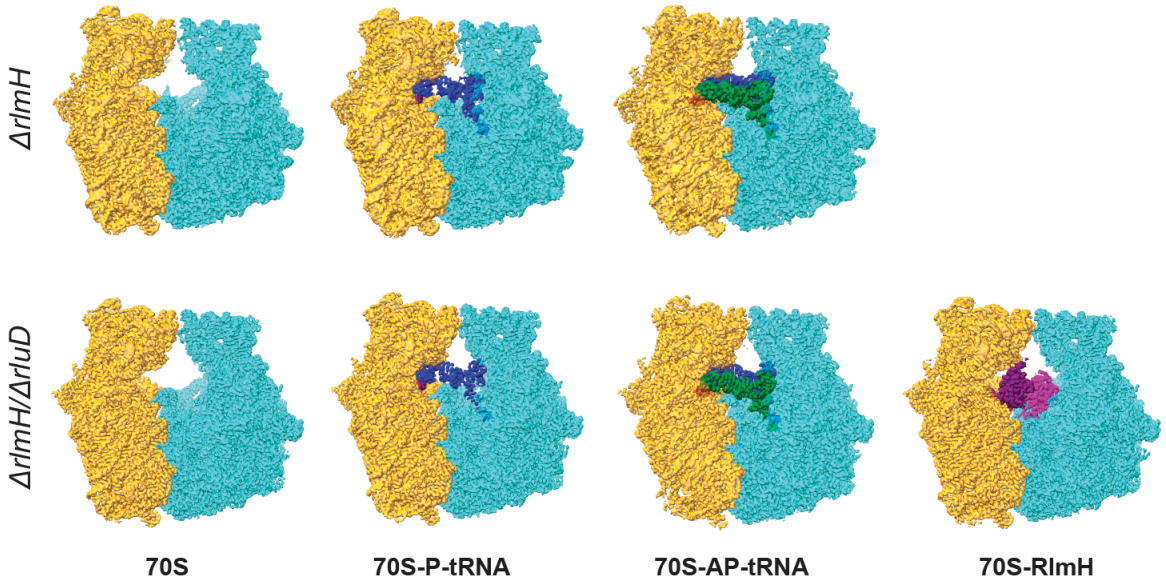

Figure S3. Distribution and classification of 70S cryo-EM electron density maps. The selected particles were divided into four main states (*ΔrlmH/ΔrluD*) or three main states (*ΔrlmH*) depending on whether RlmH is bound to the ribosome.

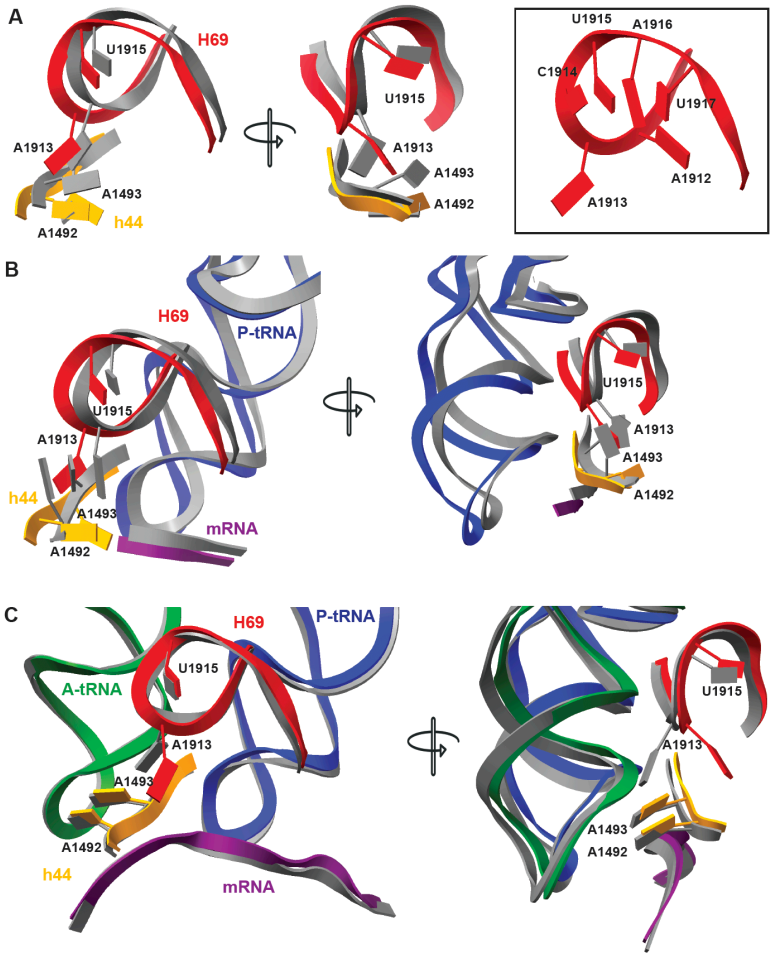

Figure S4. The effect of H69 modifications in 70S ribosomes with and without tRNA(s) and mRNA. A) Conformation of unmodified H69 in vacant ribosomes. U1915 and A1913 residues as well as h44 residues A1492 and A1493 are shown. For comparison, the conformation of H69 in the wild-type *E. coli* vacant ribosome crystal structure (PDB: 4YBB) (55) is shown in gray. **B)** Conformation of unmodified H69 in ribosomes with tRNA in the P-site. For comparison, the same region in the cryo-EM structure of 70S with initiator fMet-tRNA in the P-site (PDB ID: 9FBV) (56) is shown in gray. **C)** Conformation of unmodified H69 in ribosomes with both A- and P-site tRNAs. For comparison, the cryo-EM structure of 70S with cognate lysine tRNA in the A-site and deacylated initiator tRNA in P-site (PDB ID: 8BF7) (57). H69 is shown in red with U1915 and A1913 residues shown and labeled. Small subunit h44 residues involved in inter-subunit bridge B2a formation are shown in yellow. The A- and P-site tRNAs are shown in green and blue, respectively, and mRNA is shown in purple. A rotated view is shown for clarity. Structures are compared based on superposition of corresponding 23S rRNA molecules.

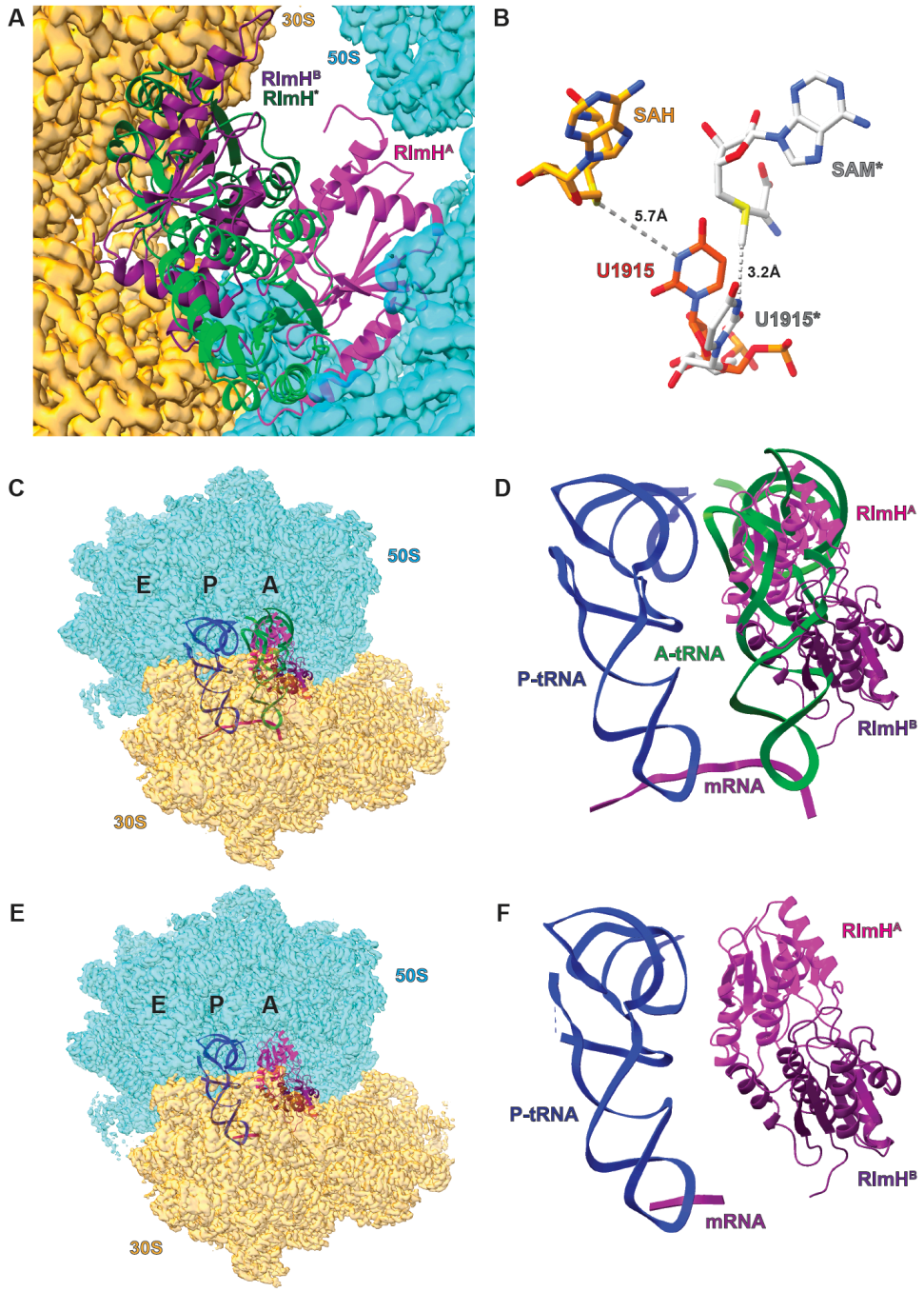

Figure S5. RlmH dimer binding mode to 70S ribosomes. A) RlmH dimer binding based on cryo-EM (magenta/purple) is different from docking simulation (lime green) (20). **B)** Substrate base and cofactor orientation in cryo-EM structure compared to docking simulation (20) (shown in gray). Distances between the uridine 1915 N1 position and the cofactor are shown in dashed lines. Note that SAH lacks the methyl group. **C-F)** Ribosome-bound RlmH does not overlap with tRNA occupying the P-site based on super positioning with PDB: 8BF7 (**C and D**) and PDB: 9FBV (E and F) but does significantly overlap with cognate tRNA bound to the A-site (**E and F**).

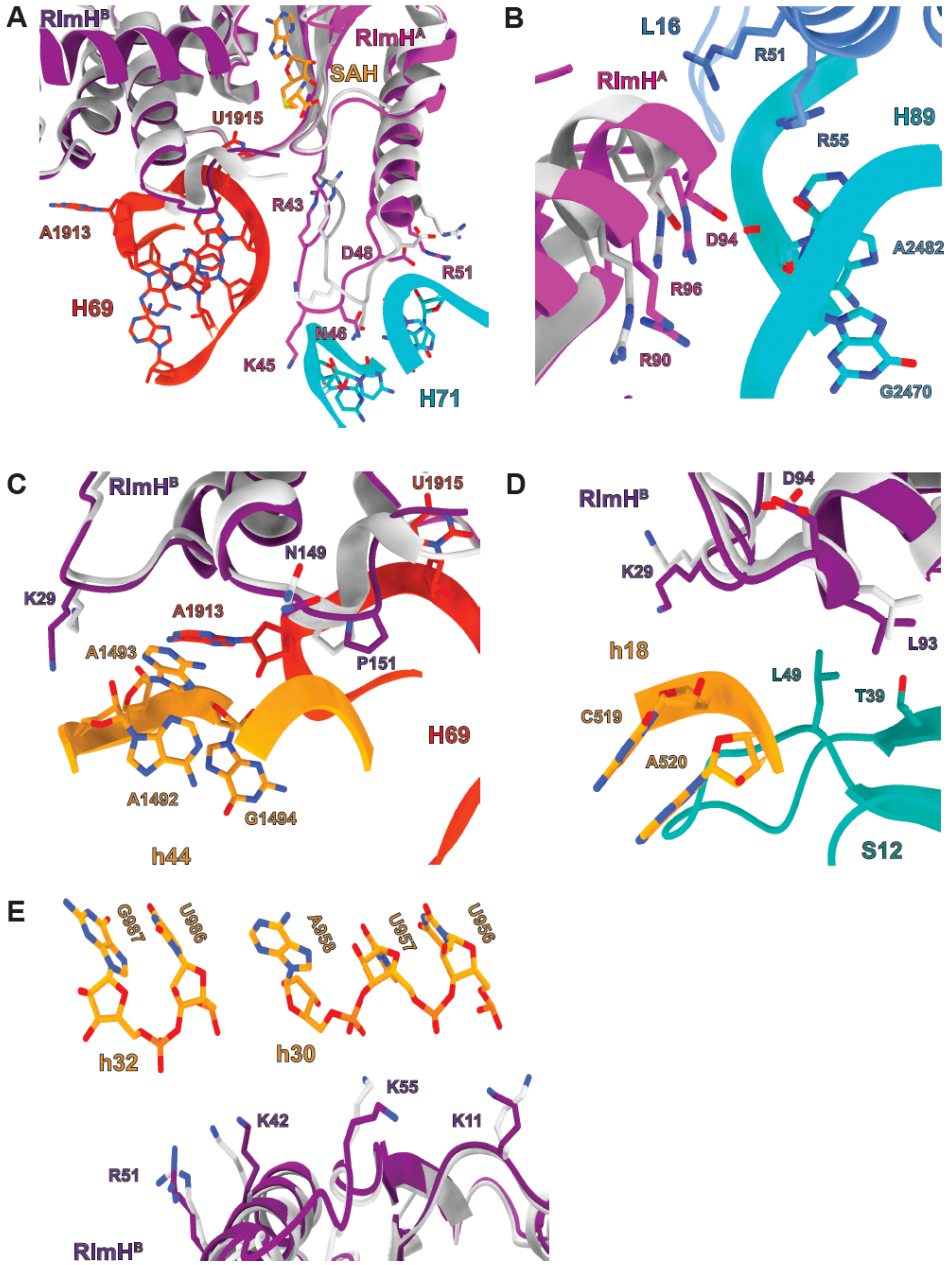

Figure S6. RlmH interactions with the ribosome. RlmH dimer interactions with 50S (shown in cyan) and 30S (shown in yellow) rRNA regions and the r-proteins L16 (light blue) and S12 (orange). For comparison, SAM-bound RlmH dimer crystal structure (PDB: 5TWJ) (superimposed based on protomer A) is shown in gray. **A)** RlmH protomer A ($RlmH^A$) interaction with H71. **B)** $RlmH^A$ interaction with H89 and the r-protein L16. **C)** $RlmH^B$ interaction with h44. **D)** $RlmH^B$ interaction with h18 and the r-protein S12. **E)** $RlmH^B$ interaction with h30 and h32. Key residues are shown in sticks and labeled.

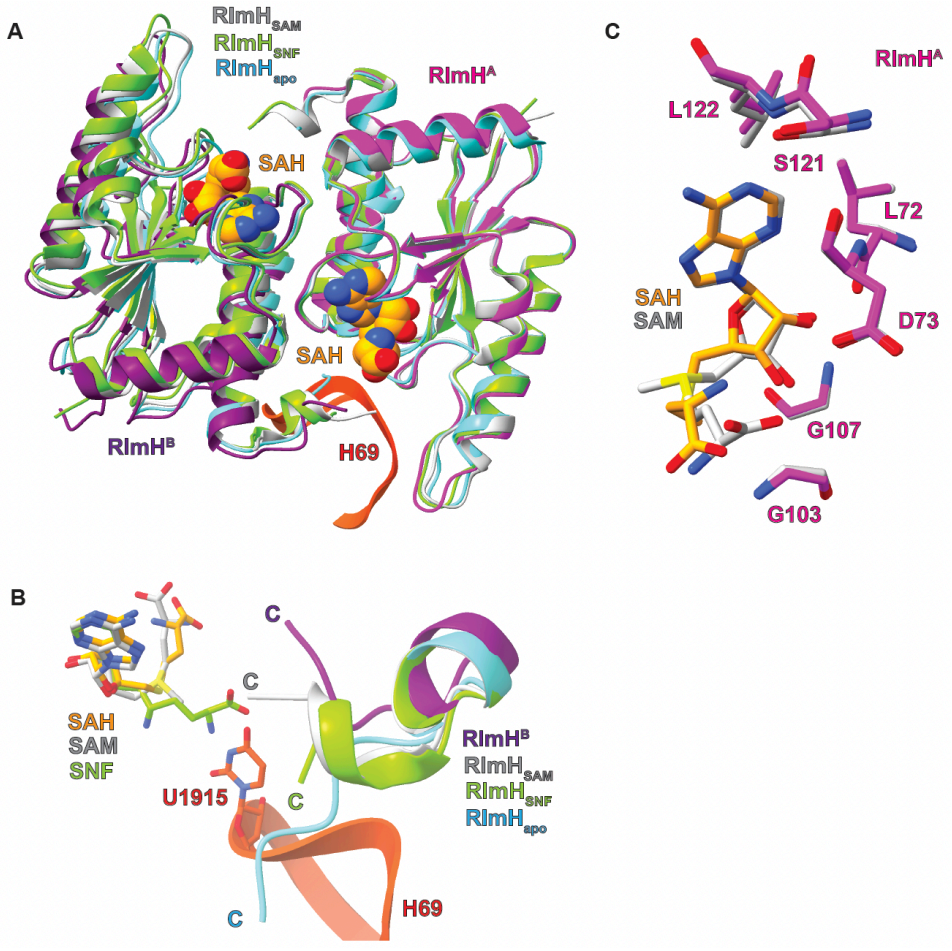

52

53 **Figure S7. RlmH cofactor binding site. A)** Comparison of the cryo-EM structure of ribosome-bound
54 RlmH-SAH, crystal structures of RlmH with SAM (PDB: 5TWJ) and sinefungin (SNF; PDB: 5TWK)
55 (29), and apo RlmH (PDB: 1NS5). Bound co-factors from current cryo-EM structure and substrate RNA
56 (base U1915 in sticks) are shown. **B)** Close-up view of the substrate and cofactor binding interface. The
57 C-terminal regions and the cofactors from available structures are shown for comparison. **C)**
58 Comparison of the cofactor binding sites of the ribosome-bound RlmH with SAH and the crystal
59 structure of RlmH with SAM (29) shown in gray. Relevant residues are shown in sticks and labeled

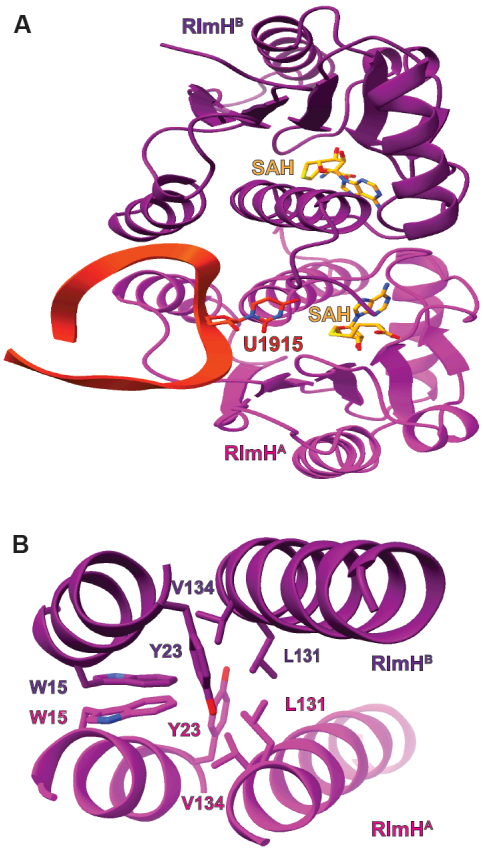

Figure S8. RlmH dimerization. A) General view of the dimerization interface of the ribosome-bound RlmH-SAH. Substrate base and SAH molecules are shown for reference. **B)** A close-up view of the dimerization interface with relevant residues shown in sticks and labeled.

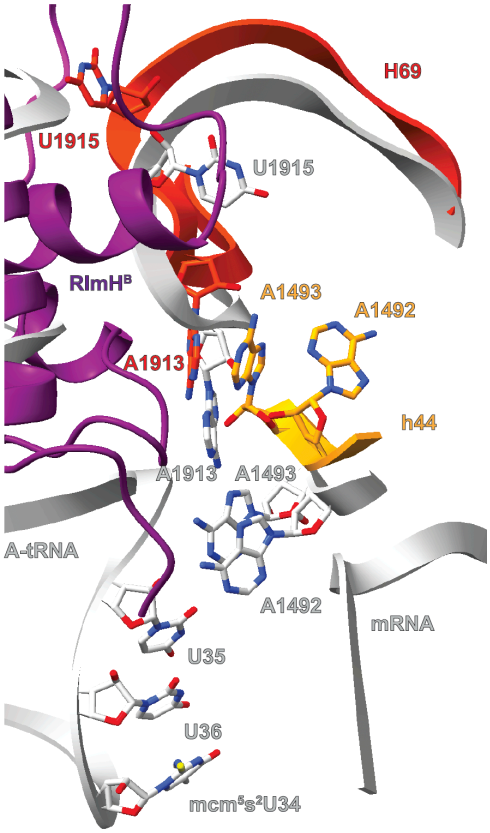

64

65 **Figure S9. RlmH binding leads to a similar conformational change in H69 A1913 as tRNA binding**
66 **to the A-site.** Comparison of unmodified H69 A1913 and h44 A1492 and A1493 in RlmH-bound
67 ribosomes to native ribosomes with cognate A- and P-site tRNAs (PDB: 8BF7) shown in gray. A-tRNA
68 anticodon bases are shown in sticks and labeled. P-site tRNA is not shown for clarity.

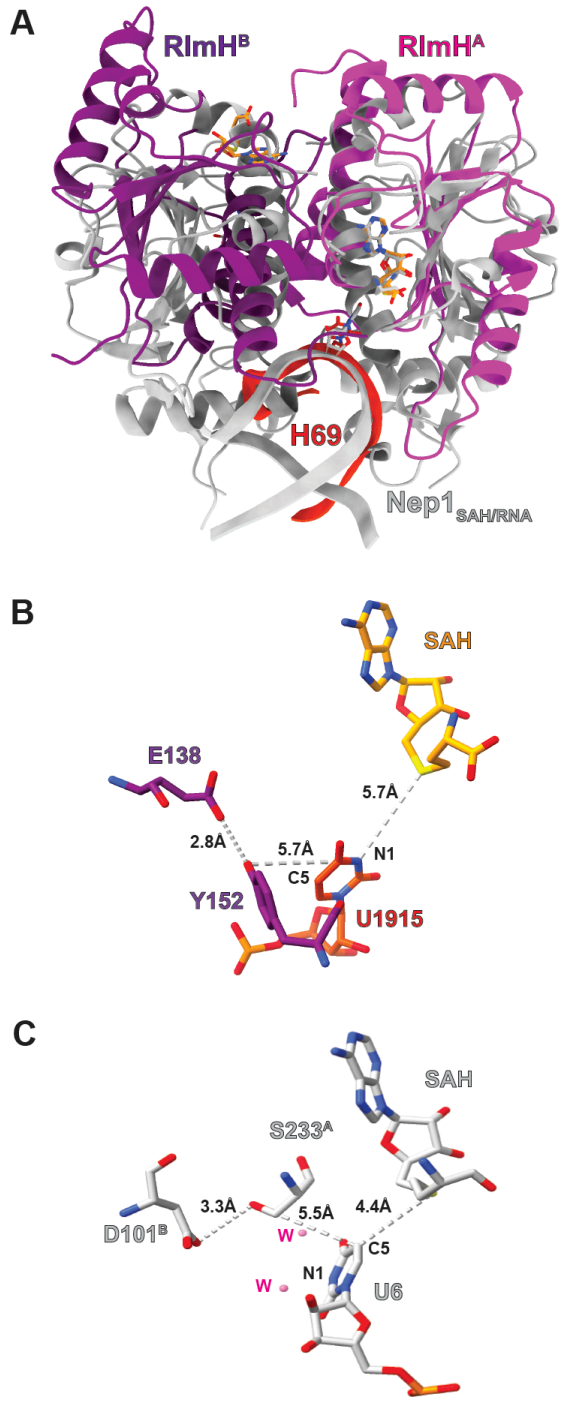

Figure S10. Comparison of the catalytic sites of RlmH and Nep1. A) Comparison of the overall conformation of substrate-bound RlmH from the current study and the yeast Nep1crystal structure (PDB: 3OIN) (32) shown in gray. Proteins are superimposed based on RlmH monomer A. Note that RlmH and Nep1 dimerize in antiparallel and perpendicular fashion, respectively. **B)** The catalytic site of RlmH with uridine. Relevant residues are shown in sticks and labeled. **C)** Same view of the catalytic site of Nep1.

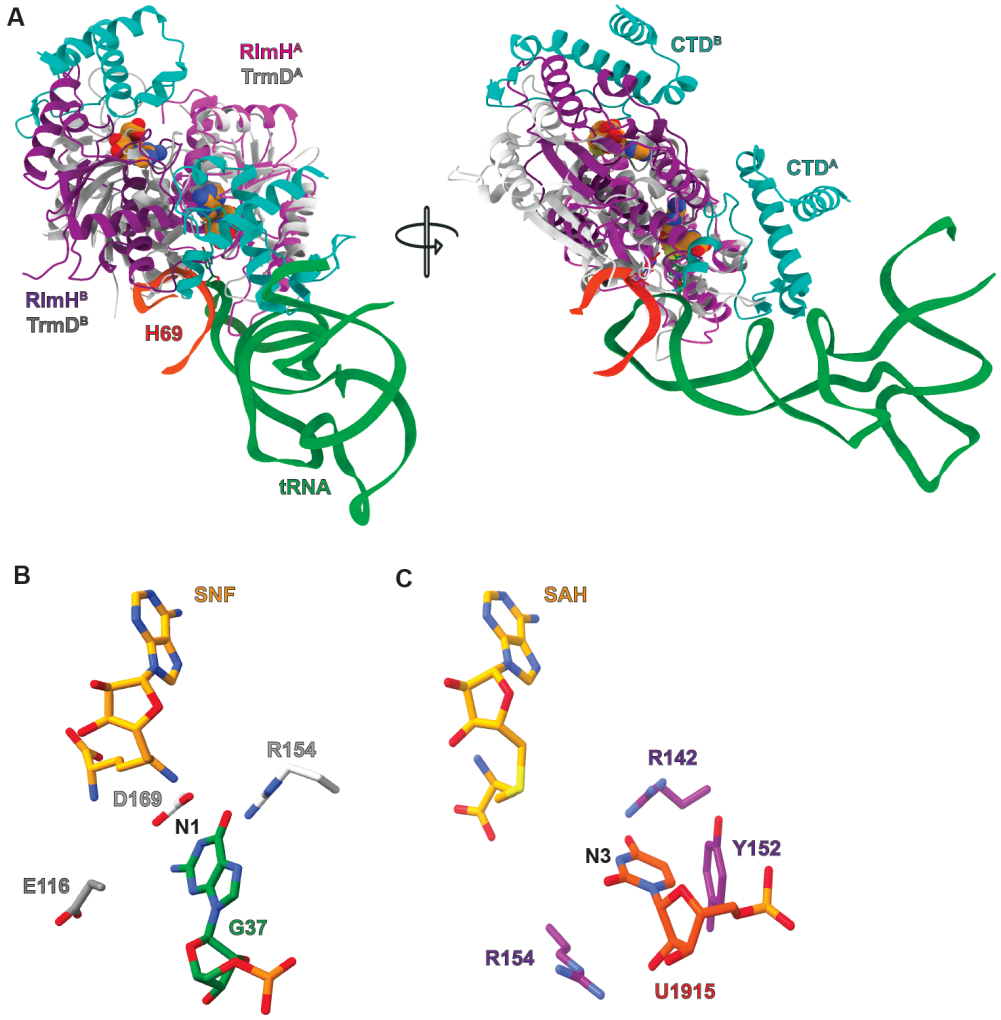

Figure S11. Comparison of the catalytic sites of RlmH and TrmD. A) Comparison of the overall conformation of substrate-bound RlmH from the current study and the crystal structure (PDB ID: 4YVI) of *Haemophilus influenzae* TrmD-sinefungin (SNF) bound to tRNA (36). Proteins are superimposed based on RlmH monomer A. Note that both RlmH and TrmD dimerize in antiparallel fashion. The C-terminal RNA binding domains (CTD) in TrmD are shown in cyan. **B)** The catalytic site of TrmD with the base flipped substrate G37. Relevant residues are shown in sticks and labeled. **C)** Same view of the catalytic site of RlmH.

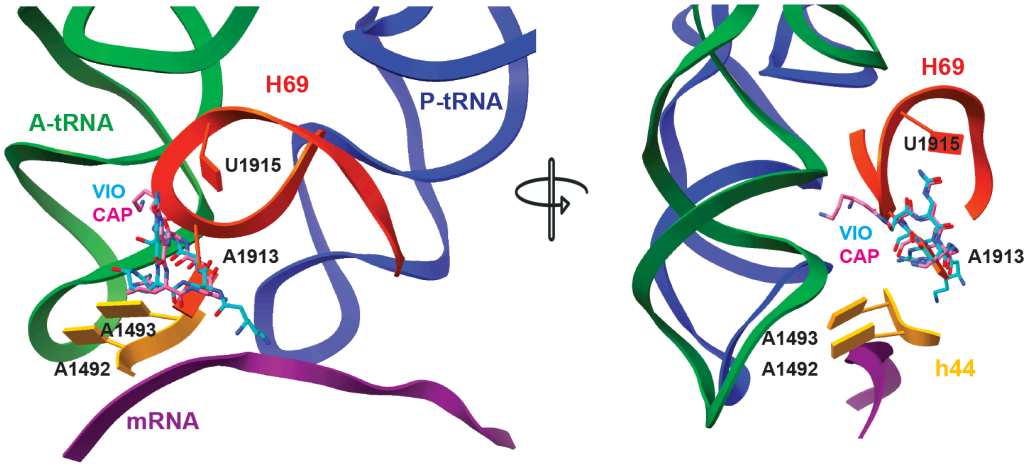

84

85 **Figure S12. Viomycin and capreomycin binding site overlaps with unmodified H69 A1913 residue**
86 **in 70S ribosomes with A- and P-site tRNAs.** Ribosome-bound viomycin (cyan) and capreomycin
87 (pink) structures (PDB ID: 4V7L and 4V7M) (52) were superimposed to *ΔrlmH/ΔrluD* 70S ribosomes
88 with A- and P-site tRNAs.

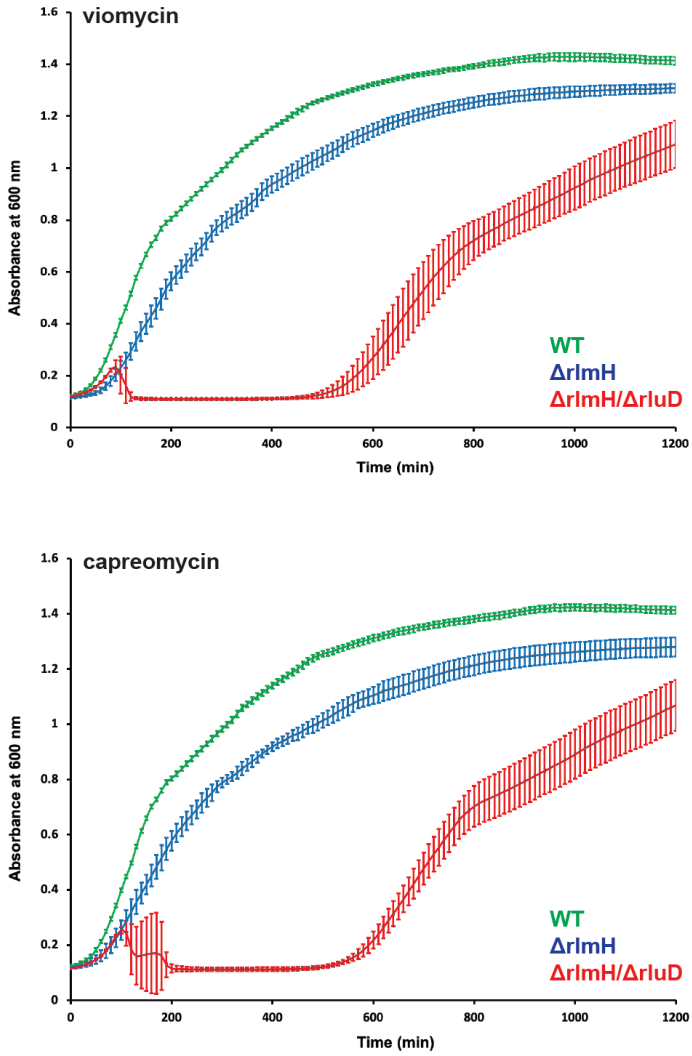

Figure S13. Growth curves of H69 modification enzyme deletion strains in the presence of tuberactinomycin. *E. coli* wild-type (WT), *rlmH* single deletion (*ΔrlmH*), and *rlmH/rluD* double deletion (*ΔrlmH/ΔrluD*) strains were grown in LB media at 37 °C in the presence of 50 μM viomycin or capreomycin. Growth curves were determined by measuring cell culture absorbance at 600 nm.